Geomorphology 475 (2025) 109665

Contents lists available at ScienceDirect

Geomorphology

journal homepage: www.journals.elsevier.com/geomorphology

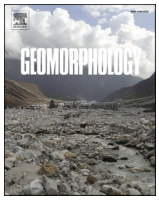

Analysis of the fundamental differences between dam-forming landslides and all landslides

Hang Wu [a,b,*], Mark A. Trigg [a], William Murphy [c], Raul Fuentes [d]

[a] School of Civil Engineering, University of Leeds, United Kingdom
[b] School of Architecture and Civil Engineering, Liming Vocational University, China
[c] School of Earth and Environment, University of Leeds, United Kingdom
[d] Institute of Geomechanics & Underground Technology, RWTH Aachen University, Germany

ARTICLE INFO

Keywords:
Landslides
Landslide dams
Global-scale
Multi-hazard

ABSTRACT

Dam-forming landslides are of significant interest to researchers, as only about 1 % of landslides block rivers, yet these dams can cause extreme flooding when they collapse, with flood flows up to ten times larger than extreme fluvial floods. While regional studies have noted differences in the dimensional characteristics and formation indices between dam-forming and non-dam-forming landslides, a global quantitative comparison has not yet been made. Using open-access global datasets, we conducted a statistical analysis of their morphometric and spatial characteristics, including volume, height/length ratio, and geomorphological factors. Spatial clustering analysis was also performed to determine whether certain landslides are more likely to form dams. The results indicate that dam-forming landslides are a distinct subset: (i) they occur in more upstream areas with higher stream power index values; (ii) they have lower mobility, confined by steeper slopes and shorter hillslope lengths; (iii) shallower landslides with larger surface area and sufficient volume are more likely to form dams; and (iv) they exhibit different spatial clustering patterns compared to general landslides. Despite some data limitations, this global study provides a foundation for quantifying a landslide dam formation index and identifying areas prone to dam formation.

1. Introduction

Landslides and landslide dams (LDams) are frequently reported worldwide, causing significant damage to infrastructure and communities (Costa and Schuster, 1988; Petley, 2012; Froude and Petley, 2018; Fan et al., 2020; Wu et al., 2022). Landslides that form dams partially or completely block fluvial channels (rivers and streams). Although only a small fraction of landslides form LDams, their impact can be severe. In Norway, 181 landslides forming LDams were recorded out of >33,000 registered landslides in the national landslide database of Norway (Oppikofer et al., 2020). A total of 828 LDams were reported among >600,000 landslides caused by the 2008 Wenchuan Earthquake, accounting for approximately 1.4 % of the total number of landslide records (Fan et al., 2012). Even though a small proportion of landslides cause river blockages, the impacts of LDams on upstream and downstream floods can be more significant than "normal" flash floods (Perucca and Angillieri, 2009). One of the most dangerous LDams triggered by the 2008 Wenchuan earthquake, the Tangjiashan LDam, caused a flood wave that reached an estimated peak discharge of 15,474 m^3/s (Xu et al., 2009), ten times the flood warning discharge of 1500 m^3/s reportedly in use by the Chengdu Water Authority (2020).

Not all the landslides would form a dam. For forming a dam, a position requires a landslide that has sufficient volume for travelling to river reach and deposition, and a river located nearby that has suitable hydrological conditions for dam formation. Although the factors related to landslides, such as landslide mass material, catchment characteristics, landslide geometry and river hydraulic conditions, are more certain, the actual mechanism for LDam formation is still under discussion (Korup, 2004; Tacconi Stefanelli et al., 2015; Fan et al., 2020; Argentin et al., 2021). A few laboratory works focus on exploring the mechanisms of LDam formation (Liao et al., 2019; Nian et al., 2020), but most focus more on analysis based on LDam records.

Korup (2002) proposed quantifying a 'scaling threshold' for river blockages to assess whether a landslide could form an LDam, using geomorphological and hydrological variables of the valley, river, and landslide. Tacconi Stefanelli et al. (2015, 2018) studied landslides and

* Corresponding author at: School of Civil Engineering, University of Leeds, United Kingdom.
E-mail address: cnhwu@leeds.ac.uk (H. Wu).

https://doi.org/10.1016/j.geomorph.2025.109665
Received 15 May 2024; Received in revised form 7 February 2025; Accepted 12 February 2025
Available online 13 February 2025
0169-555X/© 2025 The Authors. Published by Elsevier B.V. This is an open access article under the CC BY license (http://creativecommons.org/licenses/by/4.0/).

dam-forming landslides (DFLs) in specific regions, highlighting differences in landslide dimensions and valley or fluvial parameters, such as the relationship between valley width and landslide volume, and data distribution of the LDam formation index, combining landslide volume and valley width. However, thresholds calculated regionally may not be reliable when applied to other datasets or regions. Cencetti et al., 2020 showed that such an index is hard to generalize due to specific local geomorphological and hydrological conditions. Struble et al. (2021) similarly found that the dam stability index and scaling relationship between catchment area and LDam size did not align with their LDam data in Western Oregon.

A global-scale LDam formation index, or 'scaling threshold' for river blockage, has yet to be identified as the variables distinguishing blockage from non-blockage events remain unclear. Findings from a global-scale LDam dataset, RAGLAD (River Augmented Global LAndslide Dams), indicate some physical and geomorphological differences between DFLs and general landslides, particularly in geomorphological characteristics (Wu et al., 2022). In the RAGLAD dataset, the DFLs with a volume larger than 1 million cubic metres account for a larger proportion of records when compared with that of general landslide volumes. This suggests that landslide morphometric characteristics could be different between DFLs and landslides more generally. The power law scaling exponent for DFLs, based on the relationship between landslide volume and area, is smaller than that of general landslides. For global soil-slope landslides, the exponent ranges from 1.1 to 1.3, and for rock-based landslides, from 1.3 to 1.6 (Larsen et al., 2010). In contrast, the RAGLAD dataset shows DFLs have a scaling exponent between 0.66 and 0.97 (except for falls, which have an exponent of 1.52). The findings suggest that landslides forming river dams tend to have smaller volumes for a given area, likely due to DFLs developing shallower erosion depths and occurring on steeper slopes compared to typical landslides (Wu et al., 2022).

Previous research raises important questions about the key differences between landslides and DFLs. What unique properties distinguish DFLs from general landslides? Do DFLs have different mobility or size that makes them more likely to block rivers? Are their spatial distributions different? To explore these questions, we compiled global landslide and LDam records from 13 datasets, creating two subsets: one for general landslides and one for DFLs. We then systematically examined the differences between them in two main areas: (i) spatial distribution, particularly in river reaches, and (ii) landslide morphometric data, focusing on mobility (H/L ratio) and size (volume and area). These findings may help identify the necessary conditions for LDam formation, considering both landslide characteristics and the hydrological and geomorphological factors of rivers.

2. Data and Methods

2.1. Data sources of landslides and DFLs

The dimensional data of DFLs compared to general landslides show regional variations. For instance, the average impounded lake size from LDam records in New Zealand is smaller than the global average (Costa and Schuster, 1991; Korup, 2004). These regional differences in spatial distribution reflect variations in geomorphological parameters. Jibson and Harp (2012) found that the maximum epicentral distance limits for landslide occurrence were different between those landslides located in continental interiors as opposed to plate boundaries. The varied qualities of the datasets also affect the data comparison. Korup (2002) demonstrated that the impacts of the multivariate geomorphic characteristics inherent in LDam records are restricted for the quantification of data comparison. Therefore, globally consistent datasets are needed to accurately compare the differences between general landslides and DFLs globally.

However, currently, landslides do not have a well-established inventory with comprehensive and consistent data attributes, such as landslide size, on a global scale. We attempted to collect more consistent data from landslide records to cover landslide inventories from different scales and triggering mechanisms to avoid the issues caused by the scarcity of data on the specific type of landslides. For DFL records, the data is derived from the global-scale geolocated LDam dataset, RAGLAD (Wu et al., 2022). In the analysis of landslide and DFL records, different classification schemes have been employed, while global-scale datasets have consistently adopted the primary landslide classification type derived from the Varnes scheme (Varnes, 1984) or its subsequent revisions (Hungr et al., 2014).

There were 13 databases collected from local to global scales, including one mosaic database consisting of multiple event-based landslide datasets from seismically triggered landslides (Table 1). These records were either from an open-access online database or obtained with permission from the original authors or institutions. The most ideal scenario for establishing a global-scale inventory of landslides would be to collect all the event-based inventories, aiming at mapping all landslides within a single landslide-triggering episode. Several attempts have been made to establish global-scale geolocated inventories directly for landslides and LDam records (Kirschbaum, 2019; Dufresne et al., 2021; Wu et al., 2022). From these datasets, balancing the number of records against a consistent and complete dataset proves difficult.

We first categorize the data by its detail level. Fig. 1 is a schematic figure to illustrates the division of the data detail into five different levels for landslide and LDam records: level 1 - records with landslide existence reported without any reliable qualitative, quantitative, or spatial information being recorded; level 2 - geolocated records without further information; level 3 - geolocated records reported with some qualitative information such as effects or quantified data recorded qualitatively; level 4 - geolocated records reported with both qualitative information and some quantitative attributes; level 5 - geolocated records with comprehensive quantitative attributes, especially the dimension data of landslides/LDams. As the completeness of records increases, the number of records is expected to reduce. The records in the final datasets that were used for this study were assigned a detail level based on the comprehensiveness of each dataset's attributes, as shown in Fig. 1. Most of the records in the datasets are geolocated and have at least some qualitative information recorded; however, the records in level 1 were not used for further analysis due to insufficient data completeness.

It is challenging to create a comprehensive Level 5 type landslide and LDam dataset that includes precise geolocations, comprehensive landslide dimension data, and accurate landslide classifications. There are many difficulties that hinder the establishment of such a dataset, as highlighted by various landslide researchers: (i) the landslide processes are relatively isolated and need to be mapped and recorded individually, which can be laborious given the high frequency of landslide occurrence although they cover an area smaller in scale compared to floods and earthquakes (van Western et al., 2006); (ii) the majority of landslide datasets were completed by individuals or groups as part of projects and thus may not be regularly updated over time (van Western et al., 2006); (iii) landslides are a complicated hazard and contain various characteristics, thus the comprehensiveness of record attributes can be limited by factors such as access to the location (van Western et al., 2006), availability of layer-based GIS environment (Korup and Stolle, 2014), inherent incompleteness of the historical landslide records (Rossi et al., 2010), and inconsistencies in the spatiotemporal scale of triggers, drivers of landslides, and landslide models/maps (Guzzetti, 2021). For LDam dataset access, these challenges could be amplified as LDams are relatively poorly studied and most attributes in LDam records rely on existing landslide records (Fan et al., 2020; Oppikofer et al., 2020; Wu et al., 2022). Precisely geolocated LDam records, which allow further spatial analysis, require significant effort (Wu et al., 2022). Despite the relatively substantial number of LDam records available, only a small portion of LDam records can be applied for further analysis given the

Table 1
Landslide datasets and LDam datasets that were used for this study.

Index (abbreviation)	Name	Time coverage	Scale (Area)	Database format	Data coverage	Number of landslide records /events (DFL proportion)	Application in this study	Contributors
1	Landslide Inventories from An Open Repository of Earthquake-Triggered Ground-Failure Inventories	since 1900	Global	Shapefile	Earthquake-triggered landslides (event-based)	356,497(–)	Spatial distribution comparison	Schmitt et al., 2017
2	Landslide Inventories across the United States	1900–2019	National (USA)	Shapefile	Landslides-Not specific	64,433(–)	Description of landslide datasets	Jones et al., 2019
3 (Dufresne)	Dufresne (unpublished inventory)	From 270,000 B.P. (Before present)	Global	Excel	Landslides-Not specific triggers/ rockslides and rock avalanches	179 (–)	Morphometric comparison	Dufresne et al., 2021
4 (RSA-Central Asia)	Rockslides and Rock Avalanches of Central Asia	–	Regional (Central Asia)	Excel	Landslides and LDams-Not specific triggers/ rockslides and rock avalanches	1016 (19 %)	Morphometric comparison	Strom and Abdrakhmatov, 2018
5 (GLC)	Global Landslide Catalog	2007–2019	Global	Shapefile	Rainfall-triggered landslides	14,532 (–)	Spatial distribution comparison	Kirschbaum et al., 2015
6	FraneItalia	From January 2010 to 2017	National (Italy)	SQL database	Landslides-not specific	5438(single) + 1787(areal) (–)	Spatial distribution comparison	Calvello and Pecoraro, 2018
7 (HMS_LS)	High Mountain Asia Landslide Catalog V001	1956–2018	Regional (Asia)	Shapefile	Rainfall-triggered landslides	12,755 (–)	Spatial distribution comparison	Kirschbaum, 2019
8	Landslides in Dominica	–	National (Dominica)	Shapefile	Landslides- not specific	10,551(–)	Description of landslide datasets	van Westen and Zhang (2018)
9 (CAFLAG)	CAmpi Flegrei LAndslide Geodatabase	1828–2017	Local (Campi Flegrei caldera, Italy)	Shapefile	Landslides- not specific	2302 (–)	Spatial distribution comparison	Italian National Research Council (CNR) (Esposito and Matano, 2021)
10 (NIED)	Digital Archive for Landslide Distribution Maps	1981–2014	National (Japan)	Shapefile	Landslides- not specific	359,387 (–)	Morphometric comparison	National Research Institute for Earth Science and Disaster Prevention of Japan (NIED) (2014)
11(CEDIT)	Italian Catalog of Earthquake-Induced Ground Failures	1169–2019	National (Italy)	Excel	Earthquake-triggered landslides	2077 (–)	Spatial distribution comparison	Martino et al., 2022
12 (IFFI)	Italian landslide inventory	1116–2022	National (Italy)	Shapefile	Landslides-not specific	621,547(–)	Spatial distribution comparison;	IFFI, 2022; Trigila et al., 2010
13 (RAGLAD)	River Augmented Global LAndslide Dams),	Since 8 century	Global	shapefile	LDam-not specific	779 (100 %)	Morphometric comparison and Spatial distribution comparison	Wu et al., 2022

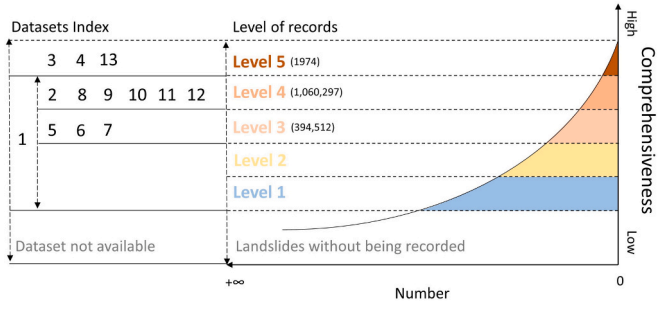

Fig. 1. Schematic graph illustrating the different levels of details of datasets for the landslide and LDam records used in this study. Levels 1 to 5 represent the five different levels of data comprehensiveness. The data index on the left corresponds to the dataset number from Table 1. The numbers in parentheses next to each level label indicate the approximate total number of records in each level used in this study.

comprehensiveness of related attributes. For instance, only 265 out of 1038 LDam records in New Zealand reported by Morgenstern et al. (2023), were utilized to analyse dam stability and breaching in detail.

After assembling the records of all the separate datasets, their data fields were unified, specifically the geospatial references to WGS 1984, as well as units and data formats. There are >1,400,000 landslide records in total, with >90 % of records containing coordinates. We retained the most complete record in cases where duplicates from various data sources shared the same spatial coordinates (approximately 1000 records were found duplicated, <0.1 % of all records). Fig. 2 illustrates the spatial distribution of mapped landslide records and LDam records from the geolocated records in the databases shown in Table 1. The landslides are geographically concentrated in the tectonically active areas, especially along the convergent plate boundaries, such as the Circum-Pacific Belt (Andes Mountains, Rocky Mountains, mountainous areas on the islands along the eastern Pacific coast, etc.) and Alpine-Himalayan orogenic belt (European Alps, Pamir Mountains, Himalayas, etc.). Landslides are also more heavily concentrated in those countries with well-established national-scale landslide inventories or

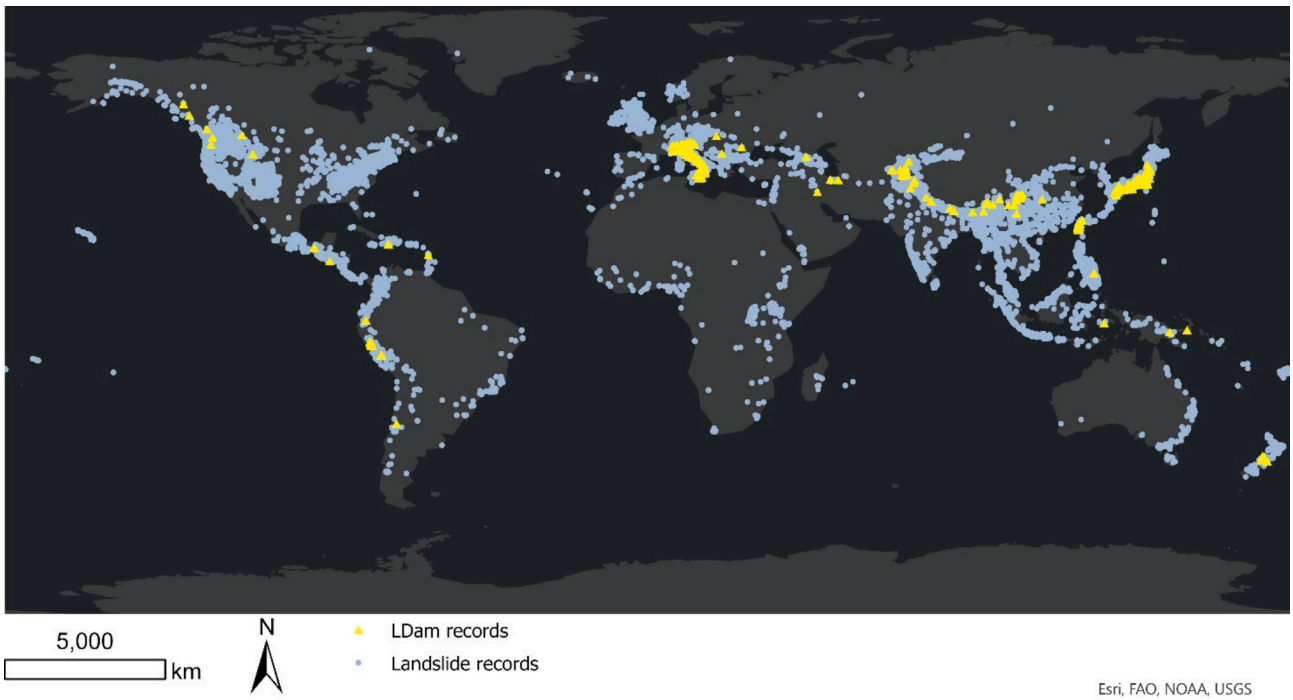

Fig. 2. Spatial distribution of landslide records from various datasets and LDam records with precise geospatial locations in RAGLAD.

extensive landslide research, such as Norway, Italy, Japan, China, India, New Zealand, and the USA. LDam records are distributed in similar locations, but as they comprise fewer records from currently available datasets, the specific focus of researchers may play an important role in the LDam record clusters.

2.2. Methods and data for comparison

2.2.1. Spatial distribution differences

There is strong evidence that LDams tend to form in tributary and headwater basins with small upstream areas, supported by both global-scale (Costa and Schuster, 1988; Fan et al., 2020; Wu et al., 2022) and regional-scale studies (Korup, 2002). Previous research has focused on global landslides causing fatalities (Petley, 2012; Froude and Petley, 2018) and regional hazards from single landslide episodes (Borgomeo et al., 2014; Dai et al., 2011). However, our study is the first to quantitatively compare the spatial distribution of landslides and DFLs on a large scale.

To minimize bias from the scarcity of LDam records in some areas, we focused on Italy and Japan, which have robust datasets. Italy and Japan can be considered as globally represent landslide and LDam data profiles due to their exceptional data density and environmental

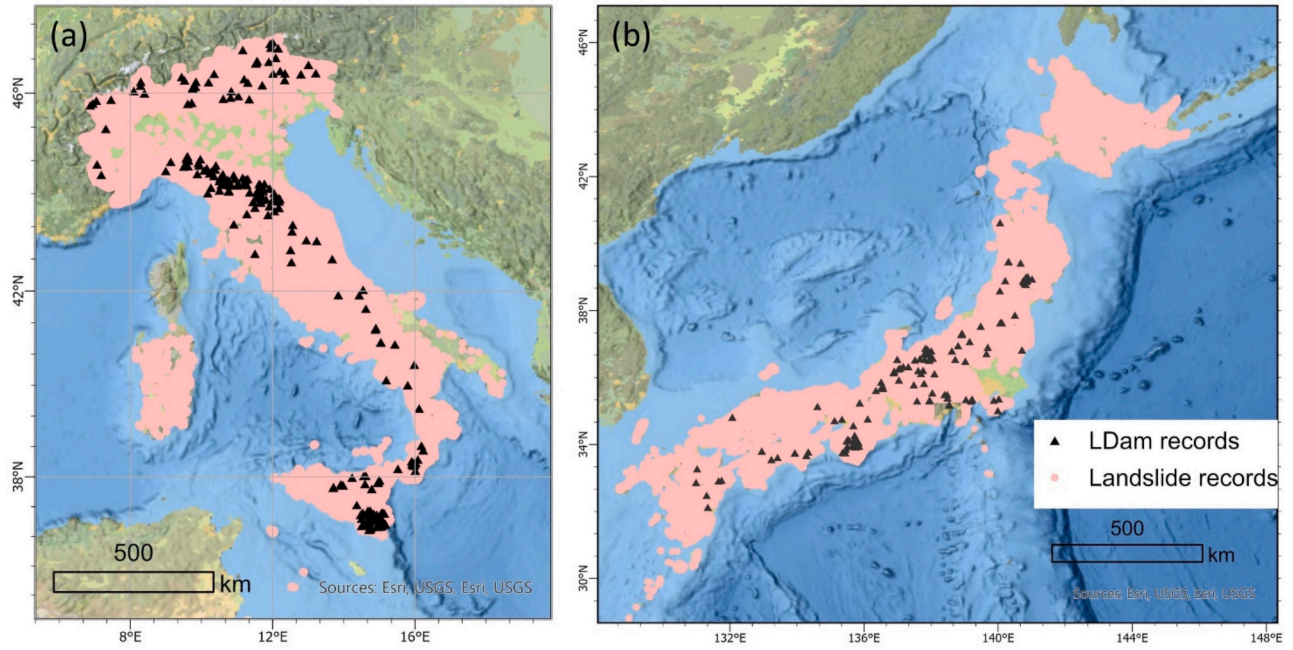

Fig. 3. LDam and landslide records that were used for the spatial distribution comparison: a) Italy; b) Japan.

diversity, making them microcosms of global landslide and LDam dynamics. They are respectively located in Alpide earthquake belt and circum-Pacific seismic belt, which were two major seismic belts around the world. The landslides and LDams in Italy represented the landslides occurring in Mediterranean and temperate zones, while those in Japan showed the landslide mechanisms in monsoon-dominated and tectonically unstable areas across Asia and the Pacific. Both countries have heterogeneous terrain that are prone to landslide occurrences. Italy was selected first for studying spatial distribution differences, as it has the most records for both landslides and LDams. Over 1 million landslide records were compiled from IFFI (IFFI, 2022; Trigila et al., 2010), along with additional landslide/LDam datasets (Table 1) and 257 LDam records from RAGLAD. The spatial distribution of these records is shown in Fig. 3(a). Italy serves as a microcosm of global conditions, with diverse lithology and landforms, including limestone-dominated mountain areas in the Alps and Apennines, metamorphic formations in Calabria, and volcanic terrains. Its precipitation ranges from <800 mm annually in Sicily (Melillo et al., 2016) to over 3000 mm in the Alps (Palladino et al., 2018). Additionally, Italy is tectonically active, with compressional forces in the alpine regions and extensional tectonics in the south. Similarly, Japan was included as a study area due to its large number of landslide and DFL records—the second highest globally. It has 359,387 landslide records from the NIED national inventory (NIED, 2014) with valid landslide area data, and 171 geolocated LDam records from RAGLAD. The spatial distribution of landslides and DFLs in Japan is shown in Fig. 3(b).

We first examine the geomorphological parameters of record locations, including elevation and upstream catchment area. The development of global fluvial datasets (GFDs) over the past decade (Yamazaki et al., 2014; Allen and Pavelsky, 2018; Frasson et al., 2019; Linke et al., 2019; Yamazaki et al., 2019; Feng et al., 2022), along with geolocated landslide and LDam inventories, has made this comparison possible. While GFDs still have limitations in representing small upstream tributaries, they provide a more consistent and reliable source of river width data than empirical methods (Wu et al., 2022).

Elevation and upstream catchment area were derived from the MERIT DEM and MERIT Hydro datasets (Yamazaki et al., 2017, 2019). Since LDam records are often collected at the valley bottom (where the river is blocked) rather than the slope, we adjusted the elevation by adding the landslide height from RAGLAD to the original MERIT DEM data.

In addition to differences in landslide catchment locations, the Stream Power Index (SPI)—a parameter used to describe the potential erosion power of flow at a given point—was applied to explore distinctions between DFLs and general landslides. SPI is calculated using Eq. 1 which incorporates slope gradient ($G, ^{\circ}$) and specific upstream catchment area (CA , km^2) (Moore et al., 1991):

$$SPI = CA \times tanG \tag{1}$$

The SPI data was sourced from geomorpho90, a global dataset of geomorphometric features derived from the MERIT DEM (Amatulli et al., 2020). To reduce uncertainties from varying catchment sizes, we created a subset of SPI data with upstream catchment areas similar to those of LDams. This subset includes landslides with upstream catchment areas under 627 km^2, a threshold where ~97 % of LDam records in RAGLAD are located (median plus 2 sigma) (Wu et al., 2022).

To investigate differences in the spatial clusters of landslides and DFLs, we applied local spatial clustering analysis using the hazard record number within level 12 HydroBASIN units. Anselin Local Moran's I (Anselin, 1995), a widely used spatial clustering index in landslide studies, helps identify landslide susceptibility hotspots (Wu and Song, 2018), examine landslide occurrence patterns (Lin et al., 2017), and track changes for landslide detection (Mondini, 2017). The Local Moran's I statistic for spatial association at feature i is calculated as follows:

$$I_i = \frac{x_i - \overline{X}}{S_i^2} \sum_{j=1\ j\neq i}^{n} W_{ij}(x_j - \overline{X}) \tag{2}$$

where x_i is the attribute of given feature i, $\overline{X}$ is the mean value of corresponding attributes, W_{ij} is the spatial matrix weight between features i and j, and:

$$S_i^2 = \frac{\sum_{j=1\ j\neq i}^{n} (x_j - \overline{X})^2}{n-1} \tag{3}$$

where n represents the total number of features. The results of local clustering analysis can be categorized into five types: high-high clusters (significant clusters of high Moran's I values), low-low clusters (significant clusters of low values), high-low or low-high outliers (values surrounded by contrasting values), and not significant.

To understand the spatial distribution differences between DFLs and general landslides, we examined their proximity to river reaches. The runout distance of a long-runout landslide that dams a river can be significant, making it challenging to define a specific threshold for DFL proximity. For example, the longest DFL runout in RAGLAD is 19 km, from the Kolka glacier-debris flow (Evans et al., 2009), with the mean runout distance for LDams being 3 km. These distances exceed what is typically considered "close" to a river (Wu et al., 2022). Instead of directly analysing the proportion of landslides/DFLs near rivers, we examined the proximity of DFLs and general landslides using data from multiple GFDs, including Global River Widths from Landsat (GRWL, Allen and Pavelsky, 2018), MERIT Hydro (Yamazaki et al., 2019), and Global Long-term River Width (GLOW, Feng et al., 2022). We converted all GFD data into points and merged them to represent the total river channels from these datasets. We also conducted river proximity analysis using EU-Hydro, a dataset offering photo-interpreted river networks across EEA39 countries, which includes surface water interpretations and a drainage model derived from the EU-DEM (European Environment Agency, 2020). However, none of these open-access datasets perfectly capture rivers and tributaries as they appear in reality. Fig. 4 shows an example of the differences between the datasets for river channels near Scanno, Italy. EU-Hydro includes more tributaries, derived from the DEM, while the GFDs mainly represent the primary channels of the Tasso and Sagittario Rivers, contrasting with the detailed mapping from Della Seta et al. (2017).

2.2.2. Morphometric differences

We then compared the morphometric data, including mobility and size, of landslides and DFLs by analysing their distribution from globally collected records. The H/L ratio, calculated by dividing landslide fall height (H) by travel length (L) (Fig. 5), is commonly used to measure landslide mobility (Corominas, 1996; Iverson, 1997). While other parameters like landslide velocity can also indicate mobility, we focused on the H/L ratio due to data limitations. Generally, a low H/L ratio indicates high mobility, while a high H/L ratio reflects low mobility. Landslide size, particularly volume, plays a crucial role in LDam formation. Fan et al. (2012) found that the relationship between landslide volume and river width was key to LDam formation during the 2008 Wenchuan Earthquake. Similarly, global LDam records from RAGLAD showed a potential threshold for LDam formation based on this relationship (Wu et al., 2022). Therefore, the morphometric parameters used to compare all landslides and DFLs include the H/L ratio and landslide volume.

It is important to note that landslide dimensions vary significantly by type (Corominas, 1996), making comparisons within specific types, when possible, more accurate. Given the abundance and completeness of rock avalanche and rockslide records, we compared their H/L ratio and volume using three datasets: the Dufresne dataset (179 records, Dufresne et al., 2021), RSA-Central Asia dataset (1016 records, Strom

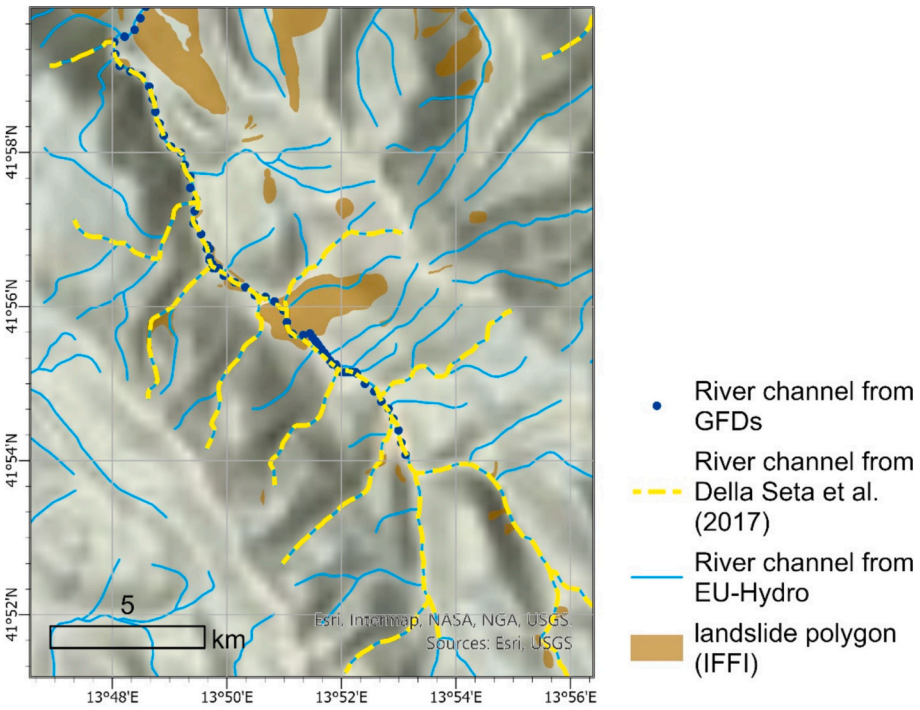

Fig. 4. The river channels represented in EU-hydro, the combination of GFDs and previous research by Della Seta et al. (2017) around Lake Scanno.

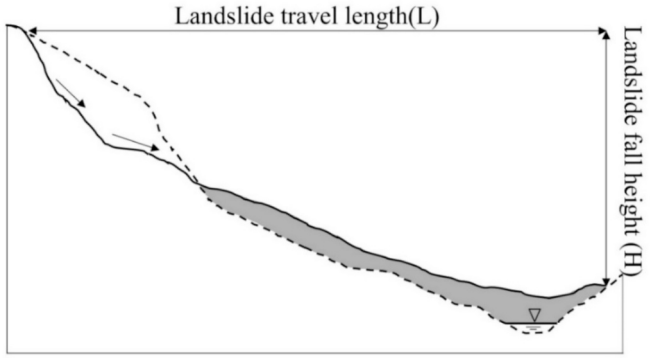

Fig. 5. Illustration of landslide fall height and travel length in H/L ratio, simplified from Fan et al. (2014).

and Abdrakhmatov, 2018), and RAGLAD dataset (779 records, Wu et al., 2022), all rated at data detail level 5. The comparison also included landslide height to assess its impact on the H/L ratio distribution. For landslide volume comparisons, records predating the Younger Dryas era (11,500 B.P.) were excluded due to potential alterations in land surface. Since many records lacked valid volume data, we also compared landslide area, as it can influence deposition and relate to LDam formation. Landslide area is a key attribute in previous LDam databases (Fan et al., 2020).

Using the described methodology, we aimed to answer three key questions regarding the mobility and size of landslides and DFLs: (i) Do DFLs exhibit higher mobility than general landslides? (ii) Do DFLs have larger volumes? (iii) Do DFLs cover larger areas? The first question addresses whether DFLs require greater mobility to reach waterbodies in sufficient volume for dam formation. The second and third questions explore whether smaller, deeper landslides (likely block movements) are more effective at forming dams than larger, shallower slides (which tend to be more fragmented).

3. Results

The data comparison assumes that if DFLs were merely a subset of general landslides, their distributions would be similar. We used box plots to compare DFLs and general landslides across geomorphological parameters such as elevation, upstream catchment area, and SPI, as well as morphometric factors like mobility and size. To explore spatial distribution differences, we conducted local spatial clustering analysis using Local Moran's I statistics. The results are presented below.

3.1. Spatial distribution differences

3.1.1. Geomorphological parameter distribution differences

We compared elevation distributions based on record locations (Fig. 6). DFLs in both Italy and Japan have higher median elevations than general landslides. The elevation distribution varied between the two countries: in Italy, DFLs showed a narrower range compared to landslides, while in Japan, the elevation range of DFLs was broader.

The comparison of upstream catchment areas showed that DFLs are more concentrated in upstream areas than general landslides. In Italy, the median upstream catchment area for DFLs is 230 km^2, compared to 289 km^2 for landslides—a difference that could result in a 36 m variation in river width, based on the relationship from Frasson et al. (2019). A similar pattern was observed in Japan, with DFLs having a median catchment area of 198 km^2, compared to 235 km^2 for landslides. Over 82 % of DFLs in Italy and 74 % in Japan were in catchments under 500 km^2, compared to 69 % of landslides in Italy and 80 % in Japan. These rivers fall under the “streams or small rivers” classification according to Bernhofen et al. (2021).

When considering both upstream catchment area and elevation distribution, it's notable that although DFLs are located in relatively upstream areas, their elevation distribution does not concentrate in higher ranges, even after elevation adjustment. DFLs in Japan exhibit a wider elevation range compared to general landslides.

DFLs in both Japan and Italy have larger SPI values compared to general landslides (Fig. 6). In Italy, the SPI distribution of the upstream subset of landslides is similar to that of DFLs but with higher values,

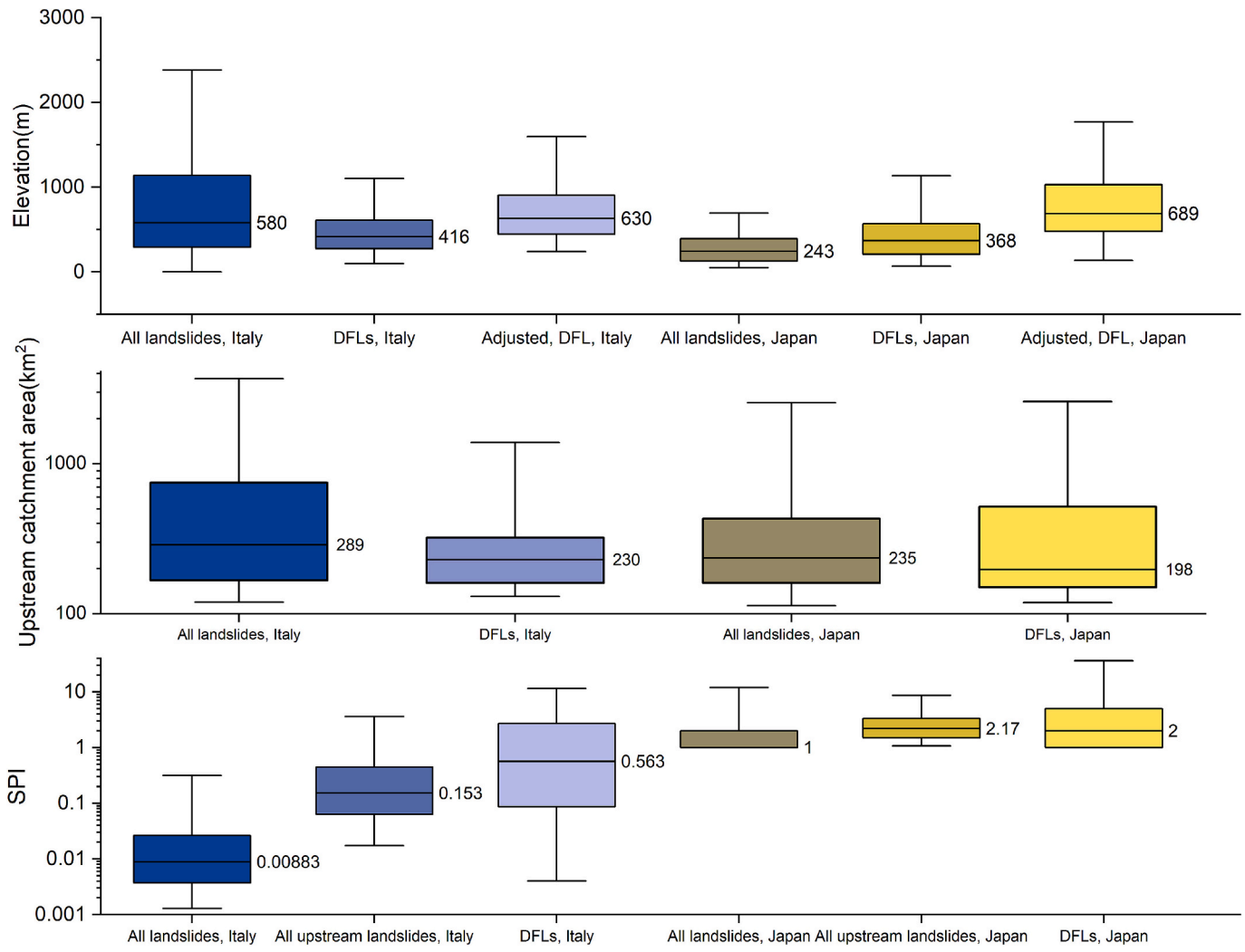

Fig. 6. Box plot showing the geomorphological parameter distribution of all landslides and DFLs in Italy and Japan.

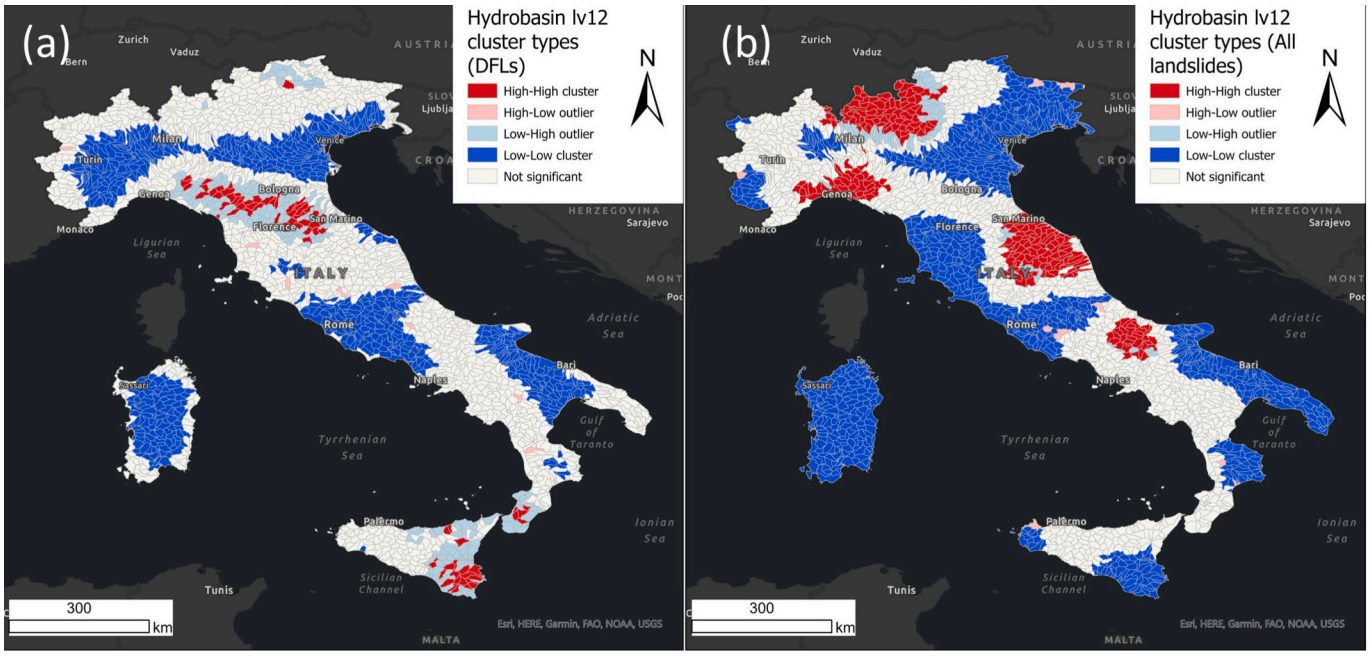

Fig. 7. Local spatial clustering analysis result of Italy: (a) DFLs (b) All landslides.

likely due to DFLs having smaller upstream catchments (Wu et al., 2022). The occurrence of river knickpoints, where the channel slope changes sharply, may also explain the high SPI in LDam formations, although the mechanism remains under discussion (Fan et al., 2020). Steep, narrow valleys require less material for dam formation, making even small landslides potential LDams in these areas. Detailed geomorphological data for Italy is available in supplementary materials section 1.1.

3.1.2. Spatial cluster differences

The spatial cluster analysis highlights hotspots for DFL and landslide occurrences, allowing us to explore differences in clustering locations. The local spatial cluster analyses for Italy and Japan (Fig. 7 and Fig. 8) show distinct high-high clusters for DFLs and general landslides. In Italy, DFL high-high clusters are found in the northern Apennine, southern Calabria, and southeastern Sicily, while landslide clusters are located in the European Alps, central Apennine, and central Liguria. Both DFLs and landslides show consistent low-low clusters in the Po Basin, Sardinia, downstream Tiber River basin, and southeastern Puglia, where the terrain is largely flat. Additional results for Italy are in supplementary materials section 1.2.

In Japan, the high-high clusters for DFLs and general landslides also showed distinct patterns. Landslide clusters are concentrated in western Hokkaido, the Hida Mountains, western Miyagi, and northern Shikoku, while DFL clusters are found in southern Nara and scattered areas around the Hida Mountains. Both DFLs and landslides share low-low clusters in the Kanto Plain, Osaka Plain, Nobi Plain, and several coastal regions.

The uniform clustering of low-low clusters in plain regions highlights the influence of local topography on landslide occurrence or absence, despite the differing high-high clusters for DFLs and general landslides in both Italy and Japan. The reasons for this difference are discussed in the following section.

3.2. Mobility and landslide size

Dufresne et al. (2021) found that rockfall/rock avalanche events generally have the smallest H/L ratios, mostly below 0.3. The RSA-Central Asia dataset (Strom and Abdrakhmatov, 2018) showed slightly higher H/L ratios, but still generally below 0.5. In contrast, the RAGLAD dataset (Wu et al., 2022) contained more records with H/L ratios exceeding 0.5 (Fig. 9). Landslides and combined landslide/DFL records tend to have H/L ratios below 0.5, consistent with values reported for general landslides (Iverson et al., 2015). Notably, RAGLAD's rock avalanche/slide records (DFLs) show higher H/L ratios, suggesting that these events travelled shorter distances before damming rivers, while those with lower H/L ratios may have lost material before reaching the river.

To expand the mobility comparison across more landslide types, we collected additional H/L ratio data from the literature (Table 2) alongside the initial three datasets. Since outliers can skew the mean, we used the median H/L ratio to minimize the influence of extreme events. The median H/L ratios of DFLs are generally larger or close to those of general landslides (with a difference of $\sim \pm 0.1$). Across various landslide types, DFLs tend to exhibit lower mobility than the wider group of landslides.

The drop height, or elevation difference between the landslide crown and deposits, is a key factor influencing the H/L ratio and landslide dynamics, such as motion and the center of gravity (Li et al., 2021). The fall height of DFLs is slightly smaller than that of general landslides, with a median height of 585 m for DFLs, compared to 950 m (Dufresne et al., 2021) and 660 m (Strom and Abdrakhmatov, 2018) in other datasets (Fig. 9). The higher H/L ratio of DFLs is likely due to their shorter runout distance, as their fall height is smaller than that of general landslides. These findings suggest that the spatial distribution of LDams is not random or simply a subset of general landslides but may be a key factor in LDam formation. The steepness of hillslopes, which influences landslide travel distance and volume, plays a crucial role in the formation of LDams.

DFLs are primarily concentrated in volumes under 5 million cubic meters and generally have smaller volumes than typical landslides (Fig. 9). A slight difference occurs for landslides exceeding 500 million cubic meters, likely due to differences in data collection focus: Dufresne et al. (2021) and Strom and Abdrakhmatov (2018) focused on landslides over 1 million cubic meters, while RAGLAD covered a broader range. If volume loss due to erosion were considered (Malamud et al., 2004), the volumes in the historical landslides dataset by Dufresne et al. (2021) and Strom and Abdrakhmatov (2018) might be larger than those in RAGLAD

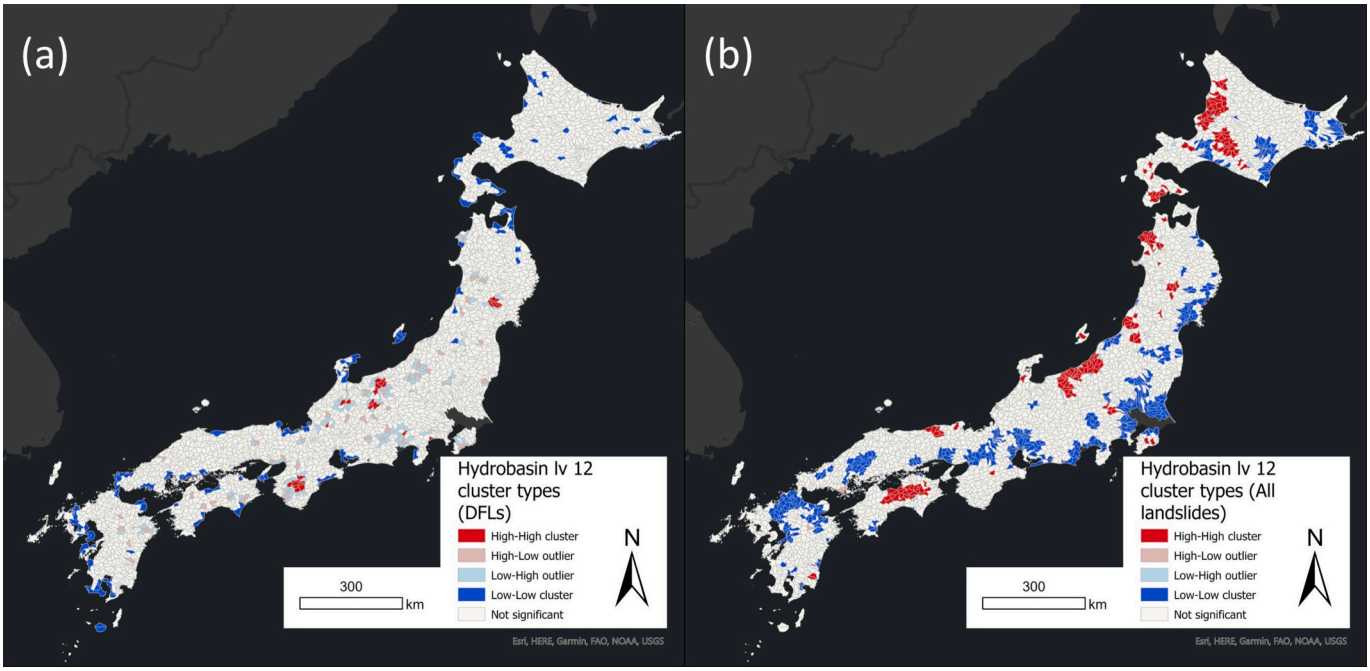

Fig. 8. Local spatial clustering analysis result of Japan: (a) DFLs (b) All landslides.

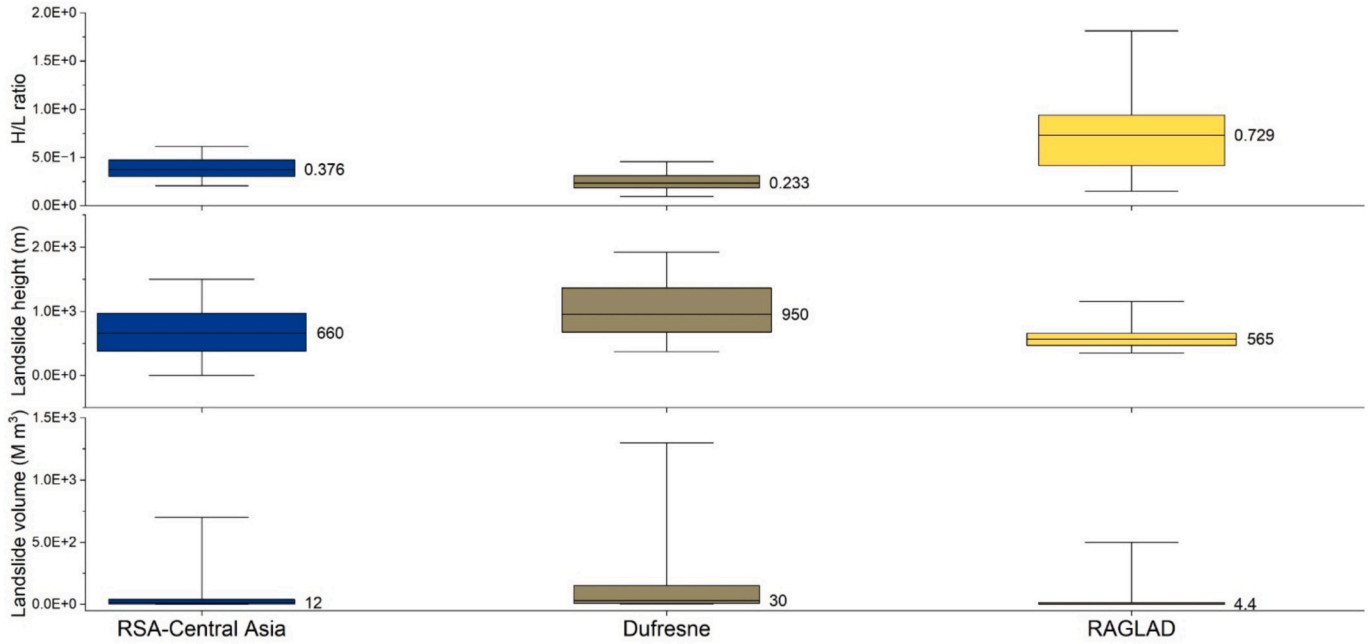

Fig. 9. Rockslide and rock avalanche morphometric parameters distributions from three different datasets: Dufresne (landslide); RSA-Central Asia (DFL/landslide combination); RAGLAD (DFL).

Table 2
H/L ratio comparison based on different landslide types in DFLs and landslides more generally, coloured by landslide type.

	Landslide type	Number of records	Min H/L ratio	Max H/L ratio	Median H/L ratio	Database/Reference (Spatial scale)
Landslides more generally	Rockslide/rock avalanche	122	0.020	0.858	0.235	Dufresne et al., 2021 (Global)
		N/A	0.083	0.929	0.641	Fan et al., 2014 (Regional)
	DFL/landslide combination – Rockslide/rock avalanche	538	0.091	0.982	0.376	Strom and Abdrakhmatov, 2018 (Regional)
	Translational/rotational slide	36	0.089	0.919	0.406	Devoli et al., 2009 (Local)
		14	0.258	0.485	0.398	Sun et al., 2021 (Local)
		N/A	0.275	1.090	0.624	Fan et al., 2014 (Regional)
	Debris flow/avalanches	65	0.052	0.739	0.467	Corominas, 1996 (Global)
		12	0.009	0.153	0.021	Capra et al., 2002 (Local)
		17	0.240	0.410	0.340	Toyos et al., 2007 (Local)
		N/A	0.205	1.025	0.528	Fan et al., 2014 (Regional)
	Earth flow	17	0.041	0.800	0.257	Corominas, 1996 (Global)
	Rockfall	45	0.117	1.087	0.664	Corominas, 1996 (Global)
		N/A	0.288	0.942	0.733	Fan et al., 2014 (Regional)
DFL	Rockslide/avalanche	21	0.150	1.930	0.804	RAGLAD (Wu et al., 2022; Global)
		N/A	0.253	0.876	0.519	Fan et al., 2014 (Regional)
	Translational/rotational slide	229	0.040	1.400	0.375	RAGLAD (Wu et al., 2022; Global)
		N/A	0.323	1.578	0.859	Fan et al., 2014 (Regional)
	Debris flow/avalanches	15	0.132	0.700	0.407	RAGLAD (Wu et al., 2022; Global)
		N/A	0.170	0.837	0.488	Fan et al., 2014 (Regional)
	Earth flow	1	0.163	–	–	RAGLAD (Wu et al., 2022; Global)
	Rockfall	14	0.011	1.534	0.443	RAGLAD (Wu et al., 2022; Global)
		N/A	0.859	1.766	1.108	Fan et al., 2014 (Regional)

(Wu et al., 2022). We also analyzed landslide area distributions in Japan with similar results (see Supplementary materials section 1.3).

We also analyzed the relationship between landslide area and frequency density for rockslides and rock avalanches to investigate size distribution (Fig. 10). For DFLs with smaller areas, around 10^5 m^2 (the roll-over point where the frequency-area distribution begins to decline), the distribution differed from the RSA-Central Asia dataset (Strom and Abdrakhmatov, 2018). This may be due to the small sample size of DFLs or the fact that smaller landslides are less likely to form dams. Another possible reason is the differing focus of datasets: Dufresne et al. (2021) emphasizes landslides larger than 1 million cubic meters, while RAGLAD (Wu et al., 2022) includes both large and small landslides.

4. Discussion

4.1. Interpretations of spatial distribution differences

4.1.1. Factors affecting the spatial clustering analysis

The spatial distribution results highlight differences in high-high spatial clusters between DFLs and general landslides. One possible reason for these differences is data collection. The clusters of general landslides in Italy and Japan are considered reliable due to the availability of multiple national-scale landslide datasets (Trigila et al., 2010; NIED, 2014; IFFI, 2022; Martino et al., 2022), and global-scale records (Schmitt et al., 2017; Kirschbaum, 2019). For DFL records, data collection bias could is likely increased due to the limitations of LDam

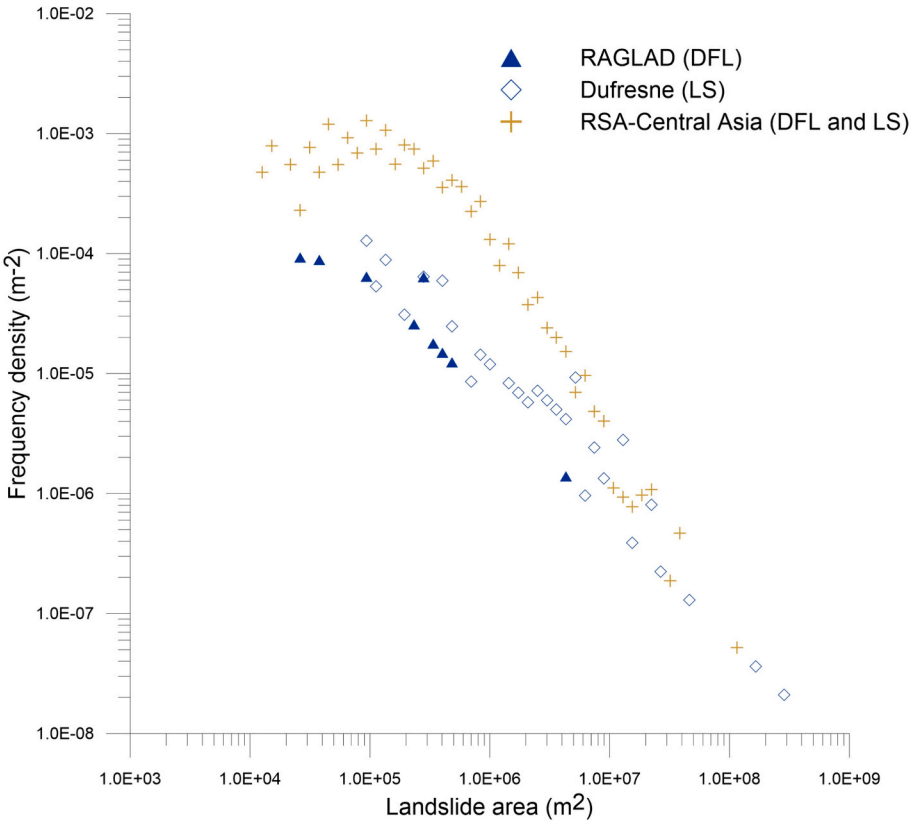

Fig. 10. Relationship of landslide frequency densities and landslide area for three datasets (Landslide type: rock avalanches and rockslides): Dufresne (landslide); RSA-Central Asia (DFL/landslide combination); RAGLAD (DFL) (LS: landslides; DFLs: Dam-forming landslides. Frequency density calculated using the same method from Tanyas et al., 2018).

record availability (Fan et al., 2020; Wu et al., 2022). Most dated LDam records in high-high cluster areas, such as southern Calabria and southeastern Sicily in Italy, and southern Nara and western Miyagi in Japan, are linked to specific extreme events, including the 1783 Calabrian earthquakes, the 1693 Sicily earthquake, the 1889 Totsukawa floods, and the 2008 Iwate–Miyagi Nairiku earthquake. However, the LDam records from the northern Apennines in Italy, and scattered regions around the Hida Mountains in Japan were collected from various events over different periods, indicating a potential difference in the spatial distribution of DFLs and general landslides. These areas are tectonic active and located in upstream mountainous regions, which provide ideal conditions for landslide occurrence and narrow receiving rivers for LDam formation.

Another factor could be the distribution of extreme hazards, such as large earthquakes and intense rainfalls, which are the primary triggers of both DFLs or general landslides globally (Costa and Schuster, 1988; Schmitt et al., 2017; Kirschbaum, 2019; Wu et al., 2022). Keefer (1984) demonstrated a correlation between the magnitude of seismic events and the area affected by landslides. Marc and Hovius (2015) found that landslide occurrence peaks after large earthquakes may be linked to the reduction and recovery of ground strength, rather than external factors such as rainfall or aftershock activity. Some high-high clusters of landslides align with areas of highest rainfall intensity across the whole country, such as Liguria (Cevasco et al., 2014), or regions of highest seismic risk, including the Apennines, Calabria and southeastern Sicily in Italy (Crowley et al., 2009), as well as southeastern Honshu Island and Shikoku in Japan (Saito et al., 2022).

4.1.2. The contribution to LDam formation of landslide occurrence and river proximity

Both landslide occurrence and river proximity are factors that could contribute to LDam formation. To assess their roles, we compared the relationship between landslide occurrence density and LDam formation, as well as the distribution of distance to rivers and LDam formation.

LDams may form in areas with higher landslide occurrence density, as formation susceptibility evaluations consider both the reactivation of existing landslides and the formation of new ones (Tacconi Stefanelli et al., 2020). Fan et al. (2012) found that the landslide occurrence density influences LDam occurrence along four cross-sections of the Min River, China. However, we did not find a strong relationship between LDam occurrence and landslide density. Using over 1 million landslide records in Italy, we mapped landslide density and extracted values at record LDam locations (Fig. 11). Many LDams were located within low-density areas, with most near only a single landslide. Similarly, when extracting density values for DFLs locations, we found they were not situated in high density areas (Fig. 12).

To assess the relationship between river proximity and LDam formation, we analyzed the distance between landslide and DFL records and the river channels, using different fluvial datasets. Similar to our adjustment of LDam elevation, we adjusted the distance to the river channels, accounting for the fact that most LDam records are located at the valley bottom rather than on the slope. We added the landslide length from RAGLAD to the extracted river distance. Both before and after the adjustment, DFLs, were located closer to river channels (Fig. 13). The distance distribution from GFD channel points for both DFLs and general landslides showed similar patterns. The distribution of distance to the EU-Hydro River channels shows a shorter distance for LDam records compared to general landslides. However, the median value of adjusted distance to rivers from EU-Hydro and GFD were 848 m and 6654 m, respectively, slightly higher than other DFL results (56 m and 5274 m, respectively), but much smaller than those of general landslides. This highlights the influence of spatial accuracy in LDam and

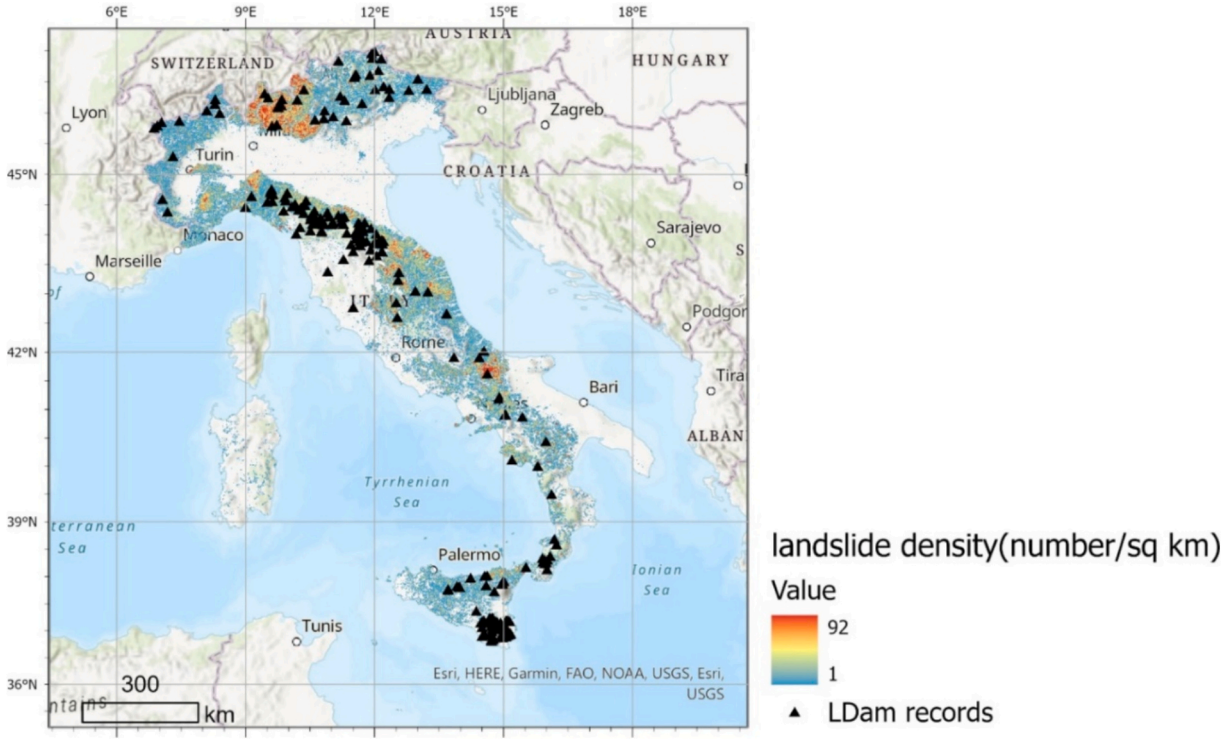

Fig. 11. LDam records and landslide density map of Italy.

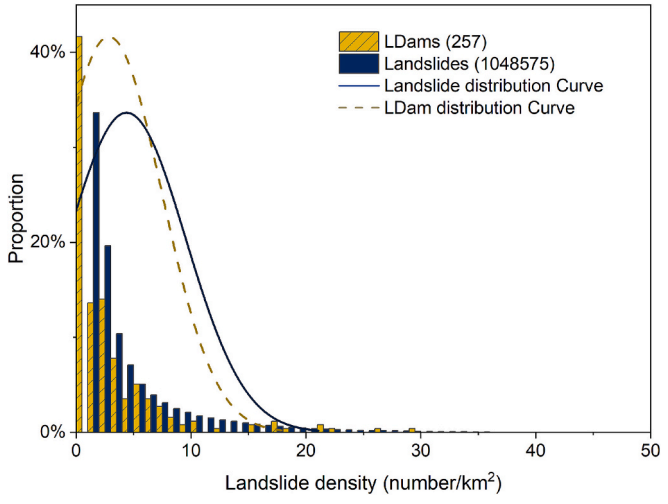

Fig. 12. Landslide density distribution at the locations of landslide records and LDam records in Italy.

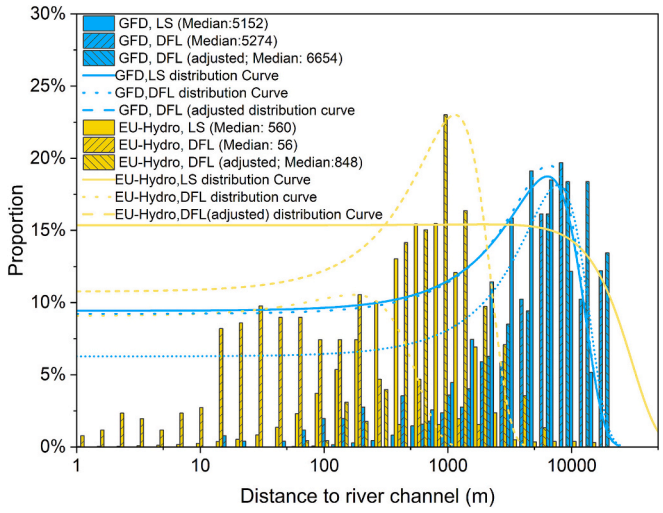

Fig. 13. Distribution of distance to river channels from either EU-hydro or a combination of GFDs for DFLs and landslides (LS). (GFD: combined global fluvial datasets, including GRWL (Allen and Pavelsky, 2018), MERIT Hydro (Yamazaki et al., 2019), and GLOW (Feng et al., 2022)).

landslide records. While were able to adjust LDam distance, general landslide records may reflect varying points (crown, center, or toe) in different datasets. Despite these location inaccuracies, our findings confirm that proximity to rivers is a crucial factor in LDam formation.

4.2. Morphometric relationship for LDam formation

We further explored the relationship between landslide volume and landslide runout length (horizontal travel distance). The data showed a distinct pattern at 2000 m (Fig. 14): for runout length <2000 m, a larger landslide volume was required to block the river; while for runout lengths >2000 m, smaller volumes could still form dams. Additionally, a clear division between landslides and DFLs is visible on the fitted curve, with a 95 % confidence band. The relationship between landslide length and volume shows strong significance coefficients (R^2) in the RSA-central Asia dataset (Strom and Abdrakhmatov, 2018) and RAGLAD (Wu et al., 2022), but not for rockslides and rock avalanches (Dufresne et al., 2021, $R^2 < 0.2$). The division suggests that the length-volume relationship could be a useful indicator for determining LDam potential, provided other conditions for LDam formation are also met. However, further exploration is needed for other types of landslides beyond rockslides and avalanches, if more data becomes available.

In summary, shallow landslides are more likely to form LDams. This is consistent with the observation of shallow slides being dam forming slides: in RAGLAD (Wu et al., 2022), the LDam materials descriptions related to fragmented material, such as debris (26.6 % of all LDam

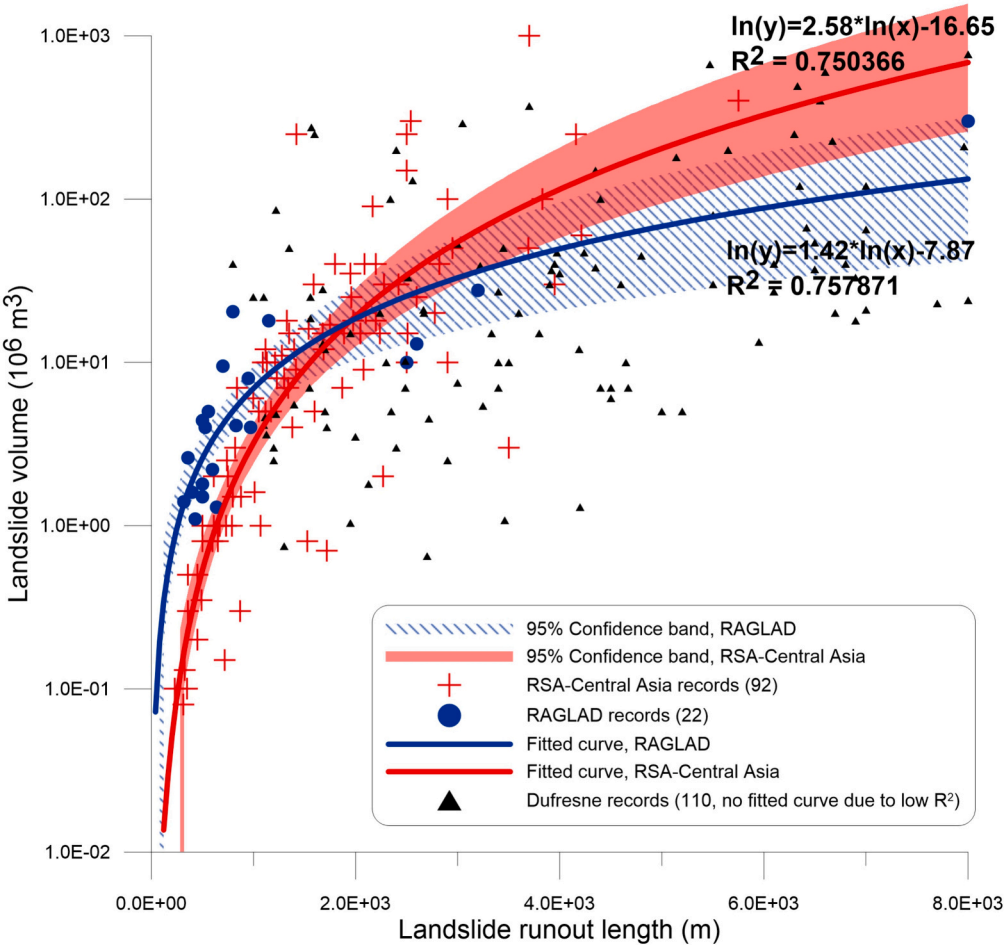

Fig. 14. Fitted curves of different landslide datasets based on the power relationship of landslide length and landslide volume (Landslide type: rock avalanches and rockslides; numbers are the sample sizes).

records) and clay (10.8 %), occur more frequently than descriptions related to obstacles, such as boulders (0.03 %) and blocks (4.2 %).

4.3. Limitations

The scarcity of landslide records, especially for DFLs, limits global-scale research due to uneven investment in research and development (R&D) across regions. Despite collecting 13 datasets from around the world, most lacked quantified morphometric data. As a result, most comparisons in this study focus on specific types of landslides, such as rock avalanches and rockslides, which offer the most reliable data for landslides and DFLs. The use of point features for landslide records highlights the challenge of calculating landslide dimensions using GIS or empirical relationships, such as volume-area (Larsen et al., 2010; Fan et al., 2014). We did not conduct further analysis as it would not alter the finding that LDams are located in more confined upstream areas than general landslides. These data limitations underscore the need for developing global fluvial datasets (GFD) and open-access, geolocated landslide inventories with comprehensive morphometric data and landslide types.

4.4. LDam formation zone

Despite the imperfections of current datasets, valuable insights can still be gained by conceptually detailing the LDam formation zone. Spatial distribution likely influences landslide morphometrics, as DFLs often occur in the upper reaches of drainage systems with smaller catchment areas. This leads to shorter runout distances and differences in mobility and size. The focus of landslide and LDam formation studies differ. LDams require specific quantification of the LDam formation zone, i.e. why the dams form at specific river reaches. Whereas general landslide research emphasizes slope conditions, such as increased shear stress, low material strength, and strength reduction (Cruden and Varnes, 1996). Therefore, it is essential to record both the DFLs and the geomorphological and hydrological characteristics of the valley at the points of river blockage (Korup, 2004; Fan et al., 2020).

Based on the differences in morphometric data and spatial distribution between DFLs and general landslides, we use a simplified schematic (Fig. 15) to show their locations along the river's longitudinal profile. The LDam formation zone, where DFLs are more likely to occur, lies between headwater regions and sediment transfer zones. These areas have steeper slopes, but within a smaller range than general landslides. The steeper, shorter slopes in upstream areas may confine landslides, limiting their size and travel distance. Hillslope length increases as the distance to the watershed outlet decreases (D'Odorico and Rigon, 2003). Since river flow magnitude and slope gradient determine stream power (Church, 2002), flow increases while slope decreases with distance from the headwaters. The SPI distribution (Fig. 5) shows that LDams form in areas with significantly higher SPI values compared to general landslides, suggesting that DFLs are located in regions with the highest SPI values along the river reaches.

For identifying LDam formation zones, key prerequisites include landslide occurrence and river presence, with river proximity being a significant factor. However, high landslide density is not necessarily required, as LDam occurrence did not strongly correlate with it. Based on this schematic figure, several geomorphological factors may help

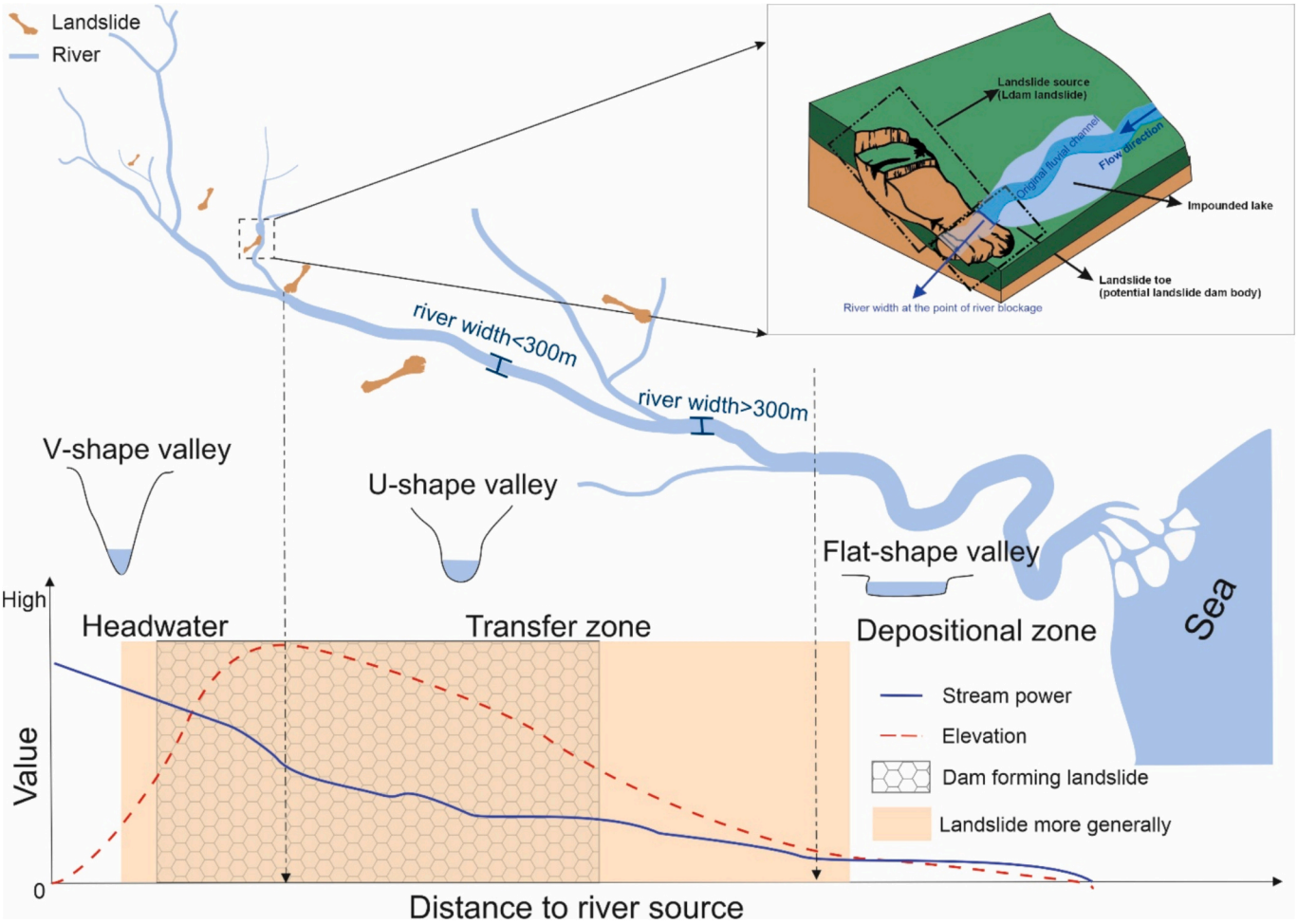

Fig. 15. Schematic figure of the LDam formation zone (stream power modified from Church, 2002).

identify potential LDam areas: headwater sediment source zones (V-shaped valleys), sediment transfer zones (U-shaped valleys), and sediment depositional zones (flat-shaped valleys), in addition to proximity to river and landslide occurrence:

1) **Elevation limitation:** Elevations either above the headwater or below the depositional area are excluded for LDam formation;
2) **River width or upstream area limitation:** Focus should be on upstream areas, as sufficiently large volumes of landslide material needed to dam the river are less common when the river width exceeds 300 m, according to RAGLAD records (Wu et al., 2022).
3) **Coastal area exclusion:** A "landslide in the coastal zone" typically refers to a landslide onto a beach or rocky shoreline, not into a river valley, and thus cannot form DFLs. Coastal areas can generally be ignored for LDam formation, as they are often depositional zones, or the landslide may cause displacement waves. However, coastal areas on mountainous islands may need to be considered due to the presence of smaller river systems.

5. Conclusions

To identify the specific characteristics of DFLs compared to landslides more generally, we collected and analyzed 13 open-access datasets. These datasets allowed us to compare differences in landslide mobility, size, and spatial distribution. The morphometric data, primarily from rock avalanches/rockslides, were drawn from the most complete datasets available. For spatial distribution, we examined geomorphological parameters like elevation, upstream catchment area, and stream power index for DFLs and landslides in Italy and Japan. We used GFDs, such as MERIT Hydro, and previously derived global-scale geomorphological datasets, such as geomorpho90, to extract relevant geomorphological characteristics. This study is the first large-scale comparison of landslide and DFL spatial distributions within a river system context.

The spatial distribution comparison shows that LDam formation locations are unique based on geomorphological parameters and local spatial cluster analysis. The result revealed that the high-high clusters of DFLs and general landslides occur in different areas, while low-low clusters overlap. DFLs are concentrated in the upstream river areas, in more laterally confined areas zones with higher SPI values compared to general landslides. This may explain the smaller landslide volume observed, as steeper hillslopes limit the landslides size. By examining landslide density and proximity to rivers, we found that proximity to rivers likely explains the spatial differences, whereas high landslide density is not a necessary condition for Ldam formation.

The comparison of landslide morphometric data shows that DFLs typically have a larger H/L ratio than general landslides, suggesting that LDams can be more easily formed by landslides with less mobility. In terms of volume and area, larger, shallower landslides are more effective at forming LDams compared to deeper landslides. There is a distinct difference in the relationships between runout distance and volume for general landslides compared to DFLs.

Based on the data distribution comparison, we propose a schematic zone along the river longitude profile to conceptually identify areas prone to LDam formation. This schematic considers factors such as the presence of landslides, river channels, river proximity, as well as fluvial

and geomorphology characteristics. The research also offers insights into selecting variables for distinguishing between river blockage and non-blockage events, highlighting the differences between DFLs and general landslides, most of which did not block rivers.

CRediT authorship contribution statement

Hang Wu: Writing – review & editing, Writing – original draft, Software, Resources, Project administration, Methodology, Funding acquisition, Formal analysis, Conceptualization. **Mark A. Trigg:** Writing – review & editing, Visualization, Supervision, Methodology, Funding acquisition, Formal analysis, Conceptualization. **William Murphy:** Writing – review & editing, Supervision, Methodology, Formal analysis, Conceptualization. **Raul Fuentes:** Writing – review & editing, Supervision, Conceptualization.

Authors' contributions

HW design the study, conducts the major jobs of data collection and analysis, and drafts the manuscript; MT, WM and RF contribute to forming the research objectives, supporting the data analyses and interpretations, and manuscript revision; HW, MT contribute to the proofreading.

Consent to participate

Not applicable for this research.

Consent for publication

Not applicable for this research.

Ethics approval

Not applicable for this research.

Funding

Hang Wu received the University of Leeds Scholarship in Associate with the China Scholarship Council (Grant no 201906400001).

Declaration of competing interest

There is no conflict of interest for this research.

Acknowledgements

Special thanks go to Dr. Anja Dufresne for providing the global-scale rockslide and rock avalanches dataset and for giving early comments on this paper; Prof. Alexander Strom for providing the rockslides and rock avalanches dataset in central Asia; Dr. Salvatore Martino and Dr. Gian Marco Marmoni for providing the updated CEDIT dataset.

Code availability

Not applicable to this research.

Appendix A. Supplementary data

Supplementary data to this article can be found online at https://doi.org/10.1016/j.geomorph.2025.109665.

Data availability

The data and other materials can be requested through the authors.

References

Allen, G.H., Pavelsky, T.M., 2018. Global extent of rivers and streams. Science 361 (6402), 585–588.
Amatulli, G., McInerney, D., Sethi, T., Strobl, P., Domisch, S., 2020. Geomorpho90m, empirical evaluation and accuracy assessment of global high-resolution geomorphometric layers. Sci Data 7 (1), 162.
Anselin, L., 1995. Local indicators of spatial association—LISA. Geogr. Anal. 27 (2), 93–115.
Argentin, A.L., Robl, J., Prasicek, G., Hergarten, S., Hölbling, D., Abad, L., Dabiri, Z., 2021. Controls on the formation and size of potential landslide dams and dammed lakes in the Austrian Alps. Nat. Hazards Earth Syst. Sci. 21 (5), 1615–1637.
Bernhofen, M.V., Trigg, M.A., Sleigh, P.A., Sampson, C.C., Smith, A.M., 2021. Global flood exposure from different sized rivers. Nat. Hazards Earth Syst. Sci. 21 (9), 2829–2847.
Borgomeo, E., Hebditch, K.V., Whittaker, A.C., Lonergan, L., 2014. Characterising the spatial distribution, frequency and geomorphic controls on landslide occurrence, Molise, Italy. Geomorphology 226, 148–161.
Calvello, M., Pecoraro, G., 2018. FraneItalia: a catalog of recent Italian landslides. Geoenviron. Disasters 5 (13), 1–16.
Capra, L., Macías, J.L., Scott, K.M., Abrams, M., Garduño-Monroy, V.H., 2002. Debris avalanches and debris flows transformed from collapses in the Trans-Mexican Volcanic Belt, Mexico - behavior, and implications for hazard assessment. J. Volcanol. Geotherm. Res. 113, 81–110.
Cencetti, C., De Rosa, P., Fredduzzi, A., 2020. Characterization of landslide dams in a sector of the central-northern Apennines (Central Italy). Heliyon 6 (6), e03799.
Cevasco, A., Pepe, G., Brandolini, P., 2014. The influences of geological and land use settings on shallow landslides triggered by an intense rainfall event in a coastal terraced environment. Bull. Eng. Geol. Environ. 859–875.
Chengdu Water Authority (2020) Analysis of flood control situation in September 2020. Chengdu Water Authority. http://cdwater.chengdu.gov.cn/cdsswj/c109454/2020-09/18/content_a00cf189c76b4188941ee3cacb815abd.shtml. Accessed 13 Nov 2022. (In Chinese).
Church, M., 2002. Geomorphic thresholds in riverine landscapes. Freshw. Biol. 47 (4), 541–557.
Corominas, J., 1996. The angle of reach as a mobility index for small and large landslides. Can. Geotech. J. 33 (2), 260–271.
Costa, J.E., Schuster, R.L., 1988. The formation and failure of natural dams. Geol. Soc. Am. Bull. 100 (7), 1054–1068.
Costa JE, Schuster RL (1991) Documented historical landslide dams from around the world (No. 91–239), https:// pubs.usgs. (gov/ of/ 1991/ 0239/report. pdf. Accessed 10 Jan 2021).
Crowley, H., Colombi, M., Borzi, B., Faravelli, M., Onida, M., Lopez, M., Polli, D., Meroni, F., Pinho, R., 2009. A comparison of seismic risk maps for Italy. Bull. Earthq. Eng. 149–180.
Cruden, D.M., Varnes, D.J., 1996. Landslide types and processes, Transportation Research Board, U.S. National Academy of Sciences, Special Report. 247, 36–75.
Dai, F.C., Xu, C., Yao, X., Xu, L., Tu, X.B., Gong, Q.M., 2011. Spatial distribution of landslides triggered by the 2008 Ms 8.0 Wenchuan earthquake, China. J. Asian Earth Sci. 40 (4), 883–895.
Della Seta, M., Esposito, C., Marmoni, G.M., Martino, S., Scarascia Mugnozza, G., Troiani, F., 2017. Morpho-structural evolution of the valley-slope systems and related implications on slope-scale gravitational processes: New results from the Mt. Genzana case history (Central Apennines, Italy). Geomorphology 289, 60–77.
Devoli, G., De Blasio, F.V., Elverhøi, A., Høeg, K., 2009. Statistical analysis of landslide events in Central America and their run-out distance. Geotech. Geol. Eng. 27, 23–42.
D'Odorico, P., Rigon, R., 2003. Hillslope and channel contributions to the hydrologic response. Water Resour. Res. 39 (5).
Dufresne, A., Siebert, L., Bernard, B., 2021. Distribution and geometric parameters of volcanic debris avalanches. In: Roverato, M, Dufresne, A, Procter, J. (Eds.), Volcanic Debris Avalanches - from Collapse to Hazards. Advances in Volcanology, Springer Heidelberg, pp. 75–90.
Esposito, G., Matano, F., 2021. CAmpi Flegrei LAndslide Geodatabase (CAFLAG). 4TU. ResearchData. Dataset. https://doi.org/10.4121/14440757.v2 (Accessed 20 Feb 2022).
European Environment Agency (2020) EU-Hydro - River Network Database, Copernicus Land Monitoring Service. https://land.copernicus.eu/imagery-in-situ/eu-hydro/eu-hydro-river-network-database?tab=metadata. Accessed 25 May 2022.
Evans, S.G., Tutubalina, O.V., Drobyshev, V.N., Chernomorets, S.S., McDougall, S., Petrakov, D.A., Hungr, O., 2009. Catastrophic detachment and high-velocity long-runout flow of Kolka Glacier, Caucasus Mountains, Russia in 2002. Geomorphology 105 (3–4), 314–321.
Fan, X., Dufresne, A., Siva Subramanian, S., Strom, A., Hermanns, R., Tacconi Stefanelli, C., Hewitt, K., Yunus, A.P., Dunning, S., Capra, L., Geertsema, M., Miller, B., Casagli, N., Jansen, J.D., Xu, Q., 2020. The formation and impact of landslide dams – State of the art. Earth Sci. Rev. 203.
Fan, X.M., van Westen, C.J., Xu, Q., Gorum, T., Dai, F.C., 2012. Analysis of landslide dams induced by the 2008 Wenchuan earthquake. J. Asian Earth Sci. 57, 25–37.
Fan, X.M., Rossiter, D.G., van Westen, C.J., Xu, Q., Gorum, T., 2014. Empirical prediction of coseismic landslide dam formation. Earth Surf Proc Land 39 (14), 1913–1926.
Feng, D., Gleason, C.J., Yang, X., Allen, G.H., Pavelsky, T.M., 2022. How have Global River Widths Changed over Time? Water Resour. Res. 58(8):e2021WR031712.
Frasson, R.P.D., Pavelsky, T.M., Fonstad, M.A., Durand, M.T., Allen, G.H., Schumann, G., Lion, C., Beighley, R.E., Yang, X., 2019. Global relationships between river width, slope, catchment area, meander wavelength, sinuosity, and discharge. Geophys. Res. Lett. 46 (6), 3252–3262.

Froude, M.J., Petley, D.N., 2018. Global fatal landslide occurrence from 2004 to 2016. Nat. Hazards Earth Syst. Sci. 18 (8), 2161–2181.
Guzzetti, F., 2021. Invited perspectives: Landslide populations – can they be predicted? Nat. Hazards Earth Syst. Sci. 21, 1467–1471. https://doi.org/10.5194/nhess-21-1467-2021.
Hungr, O., Leroueil, S., Picarelli, L., 2014. The Varnes classification of landslide types, an update. Landslides 11 (2), 167–194.
Italian Landslide Inventory (IFFI). Available online: https://www.progettoiffi.isprambiente.it/en/ (records updated on 2022, accessed on 30 December 2022).
Iverson, R.M., 1997. The physics of debris flows. Rev. Geophys. 35 (3), 245–296.
Iverson, R.M., George, D.L., Allstadt, K., Reid, M.E., Collins, B.D., Vallance, J.W., Schilling, S.P., Godt, J.W., Cannon, C.M., Magirl, C.S., Baum, R.L., Coe, J.A., Schulz, W.H., Bower, J.B., 2015. Landslide mobility and hazards: implications of the 2014 Oso disaster. Earth Planet. Sci. Lett. 412, 197–208.
Jibson, R.W., Harp, E.L., 2012. Extraordinary Distance Limits of Landslides Triggered by the 2011 Mineral, Virginia. Earthquake. Bull Seismol Soc Am 102 (6), 2368–2377.
Jones ES, Mirus BB, Schmitt RG, Baum RL, Burns WJ, Crawford M, Godt JW, Kirschbaum DB, Lancaster JT, Lindsey KO, McCoy KE, Slaughter S, Stanley TA (2019) Summary Metadata – Landslide Inventories across the United States, U.S. Geological Survey data release, doi:https://doi.org/10.5066/P9E2A37P. Accessed 20 Feb 2022.
Keefer, D.K., 1984. Landslides caused by earthquakes. Geol. Soc. Am. Bull. 95 (4), 406–421.
Kirschbaum, D.B., 2019. High Mountain Asia Landslide Catalog, Version 1. NASA National Snow and Ice Data Center Distributed Active Archive Center, Boulder, Colorado USA. https://doi.org/10.5067/5ST0TZCD9RQ3. Accessed 23 Feb 2022.
Kirschbaum, D.B., Stanley, T., Zhou, Y., 2015. Spatial and Temporal Analysis of a Global Landslide catalog. Geomorphology. https://doi.org/10.1016/j.geomorph.2015.03.016.
Korup, O., 2002. Recent research on landslide dams - a literature review with special attention to New Zealand. Prog. Phys. Geogr. 26 (2), 206–235.
Korup, O., 2004. Geomorphometric characteristics of New Zealand landslide dams. Eng. Geol. 73 (1), 13–35.
Korup, O., Stolle, A., 2014. Landslide prediction from machine learning. Geol today.30 (1):26-33.
Larsen, I.J., Montgomery, D.R., Korup, O., 2010. Landslide erosion controlled by hillslope material. Nat. Geosci. 3 (4), 247–251.
Li, H., Duan, Z., Wu, Y., Dong, C., Zhao, F., 2021. The Motion and Range of Landslides according to their Height. Front. Earth Sci. 9, 736280.
Liao, H.M., Yang, X.G., Tao, J., Zhou, J.W., 2019. Experimental study on the river blockage and landslide dam formation induced by rock slides. Eng. Geol. 261, 105269.
Lin, S.C., Ke, M.C., Lo, C.M., 2017. Evolution of landslide hotspots in Taiwan. Landslides 14, 1491–1501.
Linke, S., Lehner, B., Ouellet Dallaire, C., Ariwi, J., Grill, G., Anand, M., Beames, P., Burchard-Levine, V., Maxwell, S., Moidu, H., Tan, F., Thieme, M., 2019. Global hydro-environmental sub-basin and river reach characteristics at high spatial resolution. Sci Data 6 (1), 1–15.
Malamud, B.D., Turcotte, D.L., Guzzetti, F., Reichenbach, P., 2004. Landslide inventories and their statistical properties. Earth Surf. Process. Landf. 29 (6), 687–711.
Marc, O., Hovius, N., 2015. Amalgamation in landslide maps: effects and automatic detection. Nat. Hazards Earth Syst. Sci. 15, 723–733. https://doi.org/10.5194/nhess-15-723-2015.
Martino S, Caprari P, Fiorucci M, Marmoni GM (2022) Italian Catalogue of Earthquake-Induced Ground Failures (CEDIT), University of Rome Sapienza, https://gdb.ceri.uniroma1.it/index.php/view/map/?repository=cedit&project=Cedit Accessed 08 Sept 2022.
Melillo, M., Brunetti, M.T., Peruccacci, S., Gariano, S.L., Guzzetti, F., 2016. Rainfall thresholds for the possible landslide occurrence in Sicily (Southern Italy) based on the automatic reconstruction of rainfall events. Landslides 13, 165–172.
Mondini, A.C., 2017. Measures of spatial autocorrelation changes in multitemporal SAR images for event landslides detection. Remote Sens. 9 (6), 554.
Moore, I.D., Grayson, R.B., Ladson, A.R., 1991. Digital terrain modelling: a review of hydrological, geomorphological and biological applications. Hydrol. Process. 5, 3–30.
Morgenstern, R., Wolter, A., Cox, S.C., Lukovic, B., Bain, D., Sirohi, A., Bruce, Z., Jones, K., Rosser, B., Townsend, D., Massey, C., 2023. The New Zealand landslide dam database v1.0. Landslides, 1–14.
National Research Institute for Earth Science and Disaster Prevention of Japan, 2014. Digital archive for Landslide distribution Maps. National Research Institute for Earth Science and Disaster Prevention of Japan. https://dil-opac.bosai.go.jp/publication/nied_tech_note/landslidemap/index.html. (Accessed 23 February 2022) (in Japanese).
Nian, T.K., Wu, H., Li, D.Y., Zhao, W., Takara, K., Zheng, D.F., 2020. Experimental investigation on the formation process of landslide dams and a criterion of river blockage. Landslides 17, 2547–2562.
Oppikofer, T., Hermanns, R.L., Jakobsen, V.U., Böhme, M., Nicolet, P., Penna, I., 2020. Semi-empirical prediction of dam height and stability of dams formed by rock slope failures in Norway Nat Hazards Earth. Syst. Sci. 20 (11), 3179–3196.
Palladino, M.R., Viero, A., Turconi, L., Brunetti, M.T., Peruccacci, S., Melillo, M., Luino, F., Deganutti, A.M., Guzzetti, F., 2018. Rainfall thresholds for the activation of shallow landslides in the Italian Alps: the role of environmental conditioning factors. Geomorphology 303, 53–67.
Perucca, L.P., Angillieri, M.Y.E., 2009. Evolution of a debris-rock slide causing a natural dam: the flash flood of Rio Santa Cruz, Province of San Juan-November 12. Nat. Hazards 50 (2), 305–320.
Petley, D., 2012. Global patterns of loss of life from landslides. Geology 40 (10), 927–930.
Rossi, M., Witt, A., Guzzetti, F., Malamud, B.D., Peruccacci, S., 2010. Analysis of historical landslide time series in the Emilia-Romagna region, northern Italy. Earth Surf Proc Land 35, 1123–1137.
Saito, H., Uchiyama, S., Teshirogi, K., 2022. Rapid vegetation recovery at landslide scars detected by multitemporal high-resolution satellite imagery at Aso volcano, Japan. Geomorphology 398, 107989. https://doi.org/10.1016/j.geomorph.2021.107989.
Schmitt, R.G., Tanyas, H., Nowicki Jessee, M.A., Zhu, J., Biegel, K.M., Allstadt, K.E., Jibson, R.W., Thompson, E.M., van Westen, C.J., Sato, H.P., Wald, D.J., Godt, J.W., Gorum, T., Xu, C., Rathje, E.M., Knudsen, K.L., 2017. An Open Repository of Earthquake-Triggered Ground-Failure Inventories. Geological Survey data release collection, U.S. https://doi.org/10.5066/F7H70DB4. Accessed 23 Feb 2022.
Strom, A., Abdrakhmatov, K., 2018. Rockslides and Rock Avalanches of Central Asia - Distribution, Morphology, and Internal Structure. Elsevier.
Struble, W.T., Roering, J.J., Burns, W.J., Calhoun, N.C., Wetherell, L.R., Black, B.A., 2021. The Preservation of Climate-Driven Landslide Dams in Western Oregon. Case Rep. Med. 126 (4), e2020JF005908.
Sun, J., Wang, X., Liu, H., Yuan, H., 2021. Effects of the attitude of dominant joints on the mobility of translational landslides. Landslides 18, 2483–2498.
Tacconi Stefanelli, C., Casagli, N., Catani, F., 1635-1648. Landslide damming hazard susceptibility maps: a new GIS-based procedure for risk management. Landslides 2020.
Tacconi Stefanelli, C., Catani, F., Casagli, N., 2015. Geomorphological investigations on landslide dams. Geoenviron. Disasters 2 (1), 1–15.
Tacconi Stefanelli, C., Vilímek, V., Emmer, A., Catani, F., 2018. Morphological analysis and features of the landslide dams in the Cordillera Blanca. Peru. Landslides 15 (3), 507–521.
Tanyas, H., Allstadt, K.E., van Westen, C.J., 2018. An updated method for estimating landslide-event magnitude. Earth Surf. Process. Landf. 43 (9), 1836–1847.
Toyos, G., Dorta, D.O., Oppenheimer, C., Pareschi, M.T., Sulpizio, R., Zanchetta, G., 2007. GIS-assisted modelling for debris flow hazard assessment based on the events of May 1998 in the area of Sarno, Southern Italy: part *I*. maximum run-out. Earth Surf Processes Landforms 32 (10), 1491–1502.
Trigila, A., Iadanza, C., Spizzichino, D., 2010. Quality assessment of the Italian Landslide Inventory using GIS processing. Landslides 7, 455–470.
Varnes, D.J., 1984. Landslide Hazard Zonation: A Review of Principles and Practice. Natural Hazards, UNESCO, Paris.
van Westen C J, Zhang J (2018). Landslides and floods triggered by Huricane Maria (18 September, 2017) in Dominica. Digital or Visual Products, UNITAR-UNOSAT. http://www.unitar.org/unosat/node/44/2762 Accessed 23 May 2021.
van Westen, C., van Asch, T., Soeters, R., 2006. Landslide hazard and risk zonation—why is it still so difficult? Bull Eng Geol Environ 65, 167–184. https://doi.org/10.1007/s10064-005-0023-0.
Wu, H., Song, T., 2018. An evaluation of landslide susceptibility using probability statistic modeling and GIS's spatial clustering analysis. Hum Ecol Risk Assess. Int. J. 24 (7), 1952–1968.
Wu, H., Trigg, M.A., Murphy, W., Fuentes, R., 2022. A new global landslide dam database (RAGLAD) and analysis utilizing auxiliary global fluvial datasets. Landslides 19 (3), 555–572.
Xu, Q., Fan, X.M., Huang, R.Q., Westen, C.V., 2009. Landslide dams triggered by the Wenchuan Earthquake, Sichuan Province, south West China. Bull. Eng. Geol. Environ. 68 (3), 373–386.
Yamazaki, D., O'Loughlin, F., Trigg, M.A., Miller, Z.F., Pavelsky, T.M., Bates, P.D., 2014. Development of the Global Width Database for large Rivers. Water Resour. Res. 50 (4), 3467–3480.
Yamazaki, D., Ikeshima, D., Tawatari, R., Yamaguchi, T., O'Loughlin, F., Neal, J.C., Sampson, C.C., Kanae, S., Bates, P.D., 2017. A high-accuracy map of global terrain elevations. Geophys. Res. Lett. 44 (11), 5844–5853.
Yamazaki, D., Ikeshima, D., Sosa, J., Bates, P.D., Allen, G.H., Pavelsky, T.M., 2019. MERIT Hydro: a High-Resolution Global Hydrography Map based on latest Topography Dataset. Water Resour. Res. 55 (6), 5053–5073.